BMC Musculoskeletal Disorders

RESEARCH

Open Access

Finite element analysis of precise puncture vertebral augmentation in the treatment of different types of osteoporotic vertebral compression fractures

Hongyu Pan[1†], Hongtao Li[1†], Tianzhu Liu[3†], Changming Xiao[1†] and Sen Li[2*]

Abstract

Background Osteoporosis vertebral compression fracture (OVCF) secondary to osteoporosis is a common health problem in the elderly population. Vertebral augmentation (VA) has been widely used as a minimally invasive surgical method. The transpedicle approach is commonly used for VA puncture, but sometimes, it is limited by the anatomy of the vertebral body and can not achieve good surgical results. Therefore, we propose the treatment of OVCF with precise puncture vertebral augmentation (PPVA). This study used finite element analysis to explore the biomechanical properties of PPVA in the treatment of osteoporotic vertebral compression fractures (OVCFs) with wedge, biconcave, and collapse deformities.

Method Three-dimensional finite element models of the fractured vertebral body and adjacent superior and inferior vertebral bodies were established using Computed Tomography (CT) data from patients with OVCF, both before and after surgery. Evaluate the stress changes of the wedged deformed vertebral body, biconcave deformed vertebral body, collapsed deformed vertebral body, and adjacent vertebral bodies before and after PPVA.

Result In vertebral bodies with wedge deformity and collapsed deformity, PPVA can effectively reduce the stress on the vertebral body but increases the stress on the vertebral body with biconcave deformity. PPVA significantly decreases the stress on the adjacent vertebral bodies of the wedge deformed vertebral body, and decreases the stress on the adjacent superior vertebral body of biconcave deformity and collapsed deformed vertebral bodies, but increases the stress on the adjacent inferior vertebral bodies. PPVA improves the stress distribution of the vertebral body and prevents high-stress areas from being concentrated on one side of the vertebral body.

Conclusion PPVA has shown positive surgical outcomes in treating wedge deformed and collapsed deformed vertebral bodies. However, its effectiveness in treating biconcave vertebral body is limited. Furthermore, PPVA has demonstrated favorable results in addressing adjacent superior vertebral body in three types of fractures.

Keywords Osteoporotic vertebral compression fracture, Precision puncture vertebral augmentation, Vertebral body, Finite element analysis

†Hongyu Pan, Hongtao Li, Tianzhu Liu and Changming Xiao contributed equally to this work.

*Correspondence:
Sen Li
jht187@163.com
Full list of author information is available at the end of the article

Introduction

Osteoporosis is a systemic metabolic disease caused by the loss of calcium ions in the body, resulting in a decrease in bone density and quality [1]. Osteoporotic vertebral compression fracture (OVCF) is a prevalent secondary condition of osteoporosis, marked by intense pain, spinal deformities, and potential complications, including venous thrombosis, spinal cord injury, and infection. It seriously affects the quality of life of patients and increases the mortality rate of the elderly [2, 3]. Current treatment methods for OVCF include conservative treatment and surgical treatment, and surgical treatment is divided into open surgery and minimally invasive surgery [4]. Due to the patient's age, degree of osteoporosis, and anesthesia risk factors, open surgery usually cannot achieve the expected therapeutic effect, such as internal fixation loosening and repeated fractures. Therefore, minimally invasive surgery is usually used to treat OVCF clinically [5]. Vertebral augmentation (VA) is the primary method of minimally invasive treatment, including percutaneous kyphoplasty (PKP) and percutaneous vertebroplasty (PVP). Many surgeons use the pedicle puncture approach, the classic VA approach [6]. However, recent studies have shown that the width of the vertebral body pedicles and the coronal inclination to the vertebral body vary greatly between individuals [7]. In addition, the range of motion (ROM) of the T10-L2 vertebral body in various physiological movements of flexion and extension is more extensive in middle-aged and older women than in men, and the kyphosis angle is significantly smaller than that of men. However, after the age of 70–79, the kyphosis angle of women will increase [8]. Furthermore, Wang et al. [9] discovered that during VA on the vertebral body ranging from L1 to L5, the distance from the needle entry point to the vertebral body midline, puncture inclination, and puncture success rate were higher for the male vertebral body compared to the female vertebral body. These differences may cause the balloon and bone cement to fail to reach the anterior midline of the vertebral body during surgery, resulting in poor bone cement diffusion and unsatisfactory vertebral body reduction [10, 11]. Additionally, patients may have anatomical differences and vascular variations, so consistent use of the transpedicular approach may result in the inability of bone cement to achieve good distribution within the vertebral body, resulting in poor surgical results, or complications such as bone cement leakage, spinal cord injury, or vascular injury [12, 13]. Therefore, choosing the appropriate puncture path to repair the fractured vertebral body, reduce the stress on the vertebral body structure, and avoid intraoperative complications has become the main problem faced by clinicians [14–16]. Melton et al. [17] classified the morphological forms of vertebral fractures into wedge deformity, biconcave deformity, and collapse deformity. This classification method can cover the main compression forms of OVCF. Consequently, we propose to use precise puncture vertebral augmentation (PPVA) to treat these three types of OVCF.

The finite element analysis method is an effective discrete numerical calculation method that can perform mechanical analysis on a variety of structures and display the internal stress and deformation process when the model is stressed [18, 19]. It has been widely used in medicine and other fields, especially in bone diseases. Zhang et al. [20] used the finite element method to establish a three-dimensional model of osteoporotic adolescent scoliosis and elaborated on the stress changes of the entire lumbar segment. Zhao et al. [21] established finite element models of OVCFs vertebral bodies of different heights, analyzed their stress conditions before and after VA, and elaborated on the biomechanical effects of different types of vertebral bodies. Therefore, in order to understand the biomechanical effects of PPVA on different types of OVCFs, we used finite element modeling methods and analyzed the results, hoping to provide ideas for the clinical treatment of OVCF.

Methods

In this study, three osteoporotic thoracolumbar OVCF patients with wedge deformity, biconcave deformity, and collapse deformity fractures were selected. CT data of three patients before and after PPVA were extracted, vertebral body models before and after PPVA were established, and finite element analysis was performed. Under six physiological movements of the vertebrae, namely forward flexion, posterior extension, left bending, right bending, left rotation, and right rotation, the vertebral body stress changes of PPVA on different types of thoracolumbar OVCF were studied and used Mimics 21.0 (Belgian Materialize Company), Geomagic 2021 (scan data processing and 3D model data conversion application tool, Geomagic Company), SolidWorks 2021 (3D modeling processing software, Dassault Company), Ansys 2021R1 (finite element simulation calculation software, United States Ansys Corporation) to process the data. A CT scanner (Siemens, GER) collected raw data in DICOM format with a scan slice of 0.625 mm.

Establishment of three-dimensional geometric model

Import the DICOM files of CT scans into Mimics 21.0 for 3D model reconstruction, initial identification and separation of muscles, soft tissues, and bones. Separate each vertebral body and bone cement required into separate individuals. Due to the influence of the quality of the CT image, software, and grayscale value, repair must be performed based on the CT DICOM images of each

layer. The initially established vertebral body model was solidified, imported into an STL file and saved, and then imported into Geomagic 2021 software. All models were smoothed, spikes deleted, noise removed, and holes filled to preserve the vertebral body's characteristics. Then, the contours were drawn, the surfaces and meshes were built, the surfaces were fitted to the initially optimized model, and finally, the model was saved as a STEP entity format. To achieve the effect of the CT model, import the saved model into SolidWorks 2021 software, perform origin matching, and assemble the vertebral body. Separate the cortical bone from the cancellous bone and set the thickness of the cortical bone to 1.5 mm [22]. Save the complete three-segment vertebral body model as a part format and reconstruct the intervertebral disc(nucleus pulposus, annulus fibrosus), endplates, and articular cartilage in the model. The above software extracts reconstructs and optimizes bone cement. The generated bone cement model is saved in SLDPRT format, and the bone cement model is assembled into a vertebral body model. Assemble the separated cortical bone and cancellous bone with other vertebral structures. Finally, we obtained complete three-dimensional models before and after PPVA for wedge deformity, biconcave deformity, and collapse deformity, a total of six models (Fig. 1).

Establishment of finite element analysis model

Import the complete three-dimensional model into Ansys 2021 software to supplement the anterior longitudinal ligament, posterior longitudinal ligament, intertransverse ligament, interspinous ligament, supraspinal ligament, and ligamentum flavum. All supplementary element types support tensile deformation without compressive behavior. Based on the material properties used in previous OVCF studies (Table 1), material properties were assigned to cortical bone, cancellous bone, bone cement, endplates, cartilage, intervertebral discs (nucleus pulposus and annulus fibrosus), and various ligaments [23, 24]. The element types of cortical bone, cancellous bone, endplates, cartilage, and nucleus pulposus are defined as solid elements represented by materials with linear isotropic elasticity. The endplate, bone cement, and intervertebral disc (nucleus pulposus and annulus fibrosus) were divided into 2 mm meshes, and the articular cartilage was divided into 0.5 mm meshes [25]. According to previous literature studies, it is more reasonable when the volume unit mesh size is 0.6–1.0 mm, taking into account calculation accuracy and time.

Table 1 Finite element model component material properties

Component	Elastic modulus(Mpa)	Poisson's ratio
Osteoporotic cortical bone	8040	0.3
Cortical bone after fracture	3360	0.3
Osteoporosis cancellous bone	34	0.2
Cancellous bone after fracture	28	0.2
Endplate	23.8	0.28
Annulus fibrosus	92	0.45
Nucleus pulposus	1	0.48
Bone cement	3000	0.41
Anterior longitudinal ligament	8	0.28
Posterior longitudinal ligament	10	0.45
Intertransverse ligament	40	0.45
Interspinous ligament	12	0.45
Supraspinal ligament	12	0.45
Ligamentum flavum	20	0.45

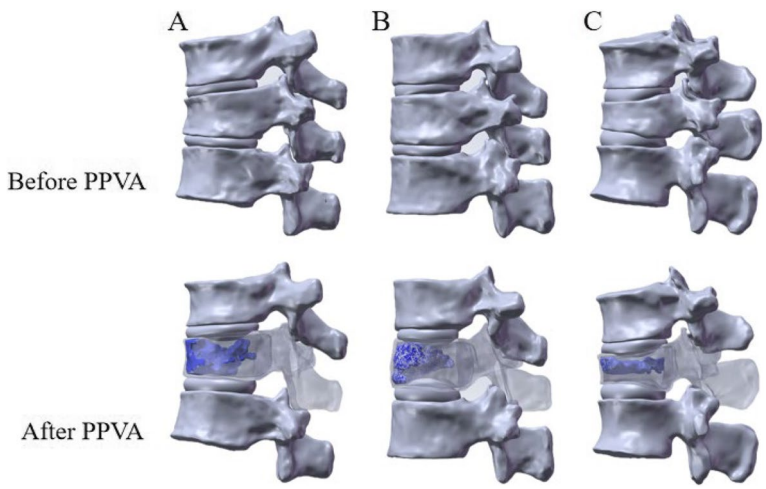

Fig. 1 Three-dimensional model of osteoporotic vertebral compression fracture. **A** wedge deformity; **B** biconcave deformity; **C** collapse deformity

Therefore, the average unit thickness of cortical bone in this article is 1 mm [26, 27]. Then set the contact type of the model components, set the articular cartilage to frictionless contact, set the cortical bone and cancellous bone, intervertebral disc and endplate, facet joint cartilage and cortical bone directly as common nodes to avoid setting contact attributes. The model was meshed using the SOLID187 ten-node tetrahedral mesh. The preoperative wedge deformity model had 151,895 elements and 253,024 nodes, and the postoperative wedge deformity model had 167,201 elements and 280,680 nodes. The preoperative biconcave deformity model had 184,439 elements and 302,582 nodes, and the postoperative biconcave deformity model had 192,011 elements and 319,370 nodes. The preoperative collapse deformity model had 233,381 elements and 379,677 nodes, and the postoperative collapse deformity model had 241,345 elements and 394,631 nodes nodes. Save the meshed model to obtain a complete finite element model (Fig. 2).

Finite element analysis

A total of six models before and after PPVA of wedge deformity, biconcave deformity, and collapse deformity were used for finite element analysis. In order to simulate the motion of the patient's thoracolumbar spine in different motion states, it is necessary to set boundary conditions and loads on the model. Constrain the mobility of all nodes on the inferior surface of the third vertebral body of the model and limit any rotation and displacement on the X, Y, and Z axes to fix the inferior surface of the third vertebral body [28]. The longitudinal axis of the spine applies a vertical pressure of 500N on the upper surface of the first vertebral body around the Z-axis. This load is evenly distributed across the entire surface to mimic the load experienced by the human thoracolumbar vertebrae in an upright position. In order to simulate the physiological movements of the human thoracolumbar vertebrae in daily activities, it is necessary to apply additional torque to the movements of the vertebrae. Apply a forward torque of 10N/m around the Y-axis to simulate the load under extension motion; Apply a reverse torque of -10N/m on the Y-axis to simulate the load under flexion motion; Apply a horizontal forward torque of 10N/m and a reverse torque of -10N/m around the X-axis to simulate the load under left and right bending, respectively; Apply a left rotation torque of 10N/m and a reverse right rotation torque of -10N/m around the Z-axis to simulate the load under left and right rotation, respectively [29–33]. According to the three-column concept of the spine, 85% of the applied pressure acts on the front and middle columns, 15% acts on the posterior columns, and the force is evenly distributed at each node [34]. Calculate the von Miese stress of three types of vertebral bodies and the von Mises stress of adjacent vertebral bodies, and evaluate the stress changes of the vertebral body after PPVA treatment.

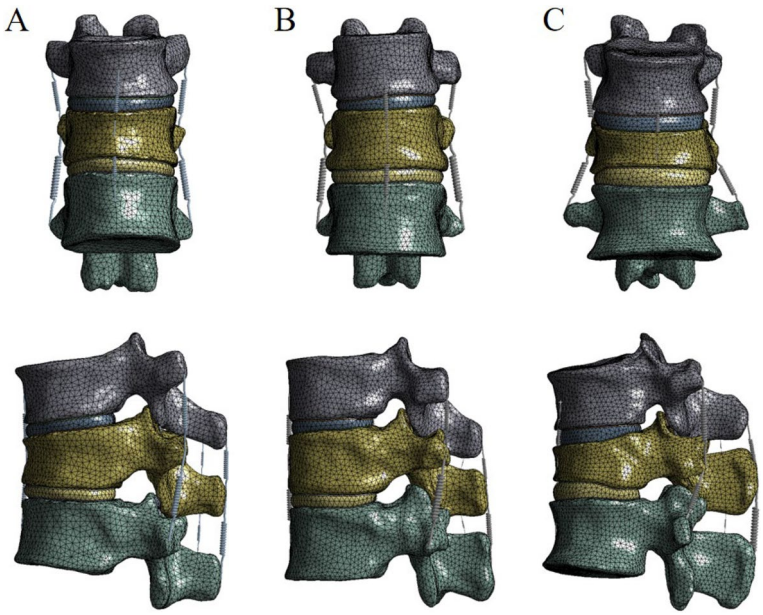

Fig. 2 Finite element analysis model for osteoporotic vertebral compression fracture. **A** wedge deformity; **B** biconcave deformity; **C** collapse deformity

Result

Wedge deformity

Stress changes in fractured vertebral body

In the wedge deformity model, the T11 vertebral body is fractured, and the adjacent vertebral bodies are the T10 and T12 vertebral bodies. The stress distribution cloud diagram of the T11, T10, and T12 vertebral bodies is shown below (Fig. 3). Under the six different physiological movements of the vertebral body, the maximum stress on the T11 vertebral body before PPVA was generated by forward flexion, which was 32.231Mpa, while the maximum stress generated was the smallest by posterior extension, which was 24.704Mpa (Table 2). The maximum stress on the T11 vertebral body after PPVA was generated by right bending, which was 21.79Mpa, while the maximum stress generated was the smallest by left bending, which was 16.967Mpa (Table 2). After PPVA, the maximum stress of the T11 wedge deformed vertebral body was significantly decreased, with forward flexion decreased by 44.22%, posterior extension decreased by 26.66%, left bending decreased by 32.69%, right bending decreased by 21.13%, left rotation decreased by 37.34%, and right rotation decreased by 35.45% (Fig. 4).

Stress changes in adjacent vertebral bodies

Under the six different physiological movements of the vertebral body, the maximum stress on the T10 vertebral body before PPVA was generated by right bending, which was 34.49Mpa, while the maximum stress was the smallest generated by left rotation, which was 27.767 (Table 2). The maximum stress on the T10 vertebral body after PPVA was generated by forward flexion, which was 33.037Mpa, while the maximum stress was the smallest generated by left bending, which was 25.128Mpa (Table 2). After PPVA, except for forward flexion, the maximum stress of adjacent vertebral body

Fig. 3 Stress distribution cloud diagram of wedge vertebral body and adjacent vertebral bodies before and after PPVA. Pre, Preoperative; Post, Postoperative

Table 2 Wedge deformity vertebral body and adjacent vertebral bodies stress before and after PPVA

	Flexion		Extension		Left bending		Right bending		Left rotation		Right rotation	
	Pre	Post	Pre	Post	Pre	Post	Pre	Post	Pre	Post	Pre	Post
T10	30.423	33.037	33.783	28.061	27.95	25.128	34.49	30.85	27.767	26.756	29.361	26.738
T11	32.231	17.98	24.704	18.117	25.209	16.967	31.638	21.79	28.281	17.72	28.466	18.374
T12	31.488	28.271	24.859	18.657	24.414	22.068	31.967	24.867	28.304	23.429	28.11	23.517

Pre Preoperative, *Post* Postoperative

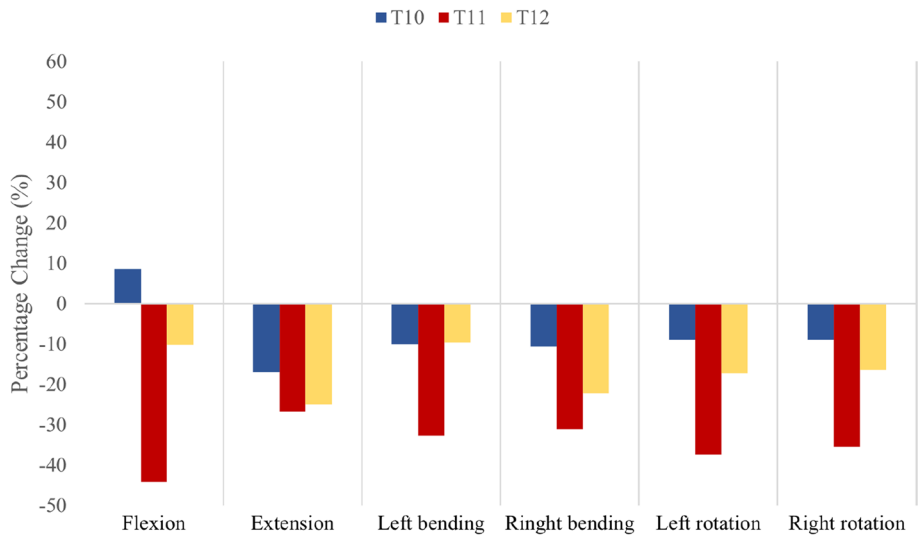

Fig. 4 Stress changes in wedge deformity vertebral body and adjacent vertebral bodies under six physiological movements after PPVA

T10 decreased to varying degrees under other different physiological movements. Forward flexion increased by 8.59%, posterior extension decreased by 16.94%, left bending decreased by 10.1%, right bending decreased by 10.55%, left rotation decreased by 3.64%, and right rotation decreased by 8.93% (Fig. 4). Under the six different physiological movements of the vertebral body, the maximum stress on the T12 vertebral body before PPVA was generated by right bending, which was 31.967Mpa, while the maximum stress was the smallest generated by left bending, which was 24.414 (Table 2). The maximum stress on the T12 vertebral body after PPVA was generated by forward flexion, which was 28.271Mpa, while the maximum stress was the smallest generated by posterior extension, which was 18.657Mpa (Table 2). After PPVA, the maximum stress of adjacent vertebral body T12 was significantly decreased, with forward flexion decreased by 44.22%, posterior extension decreased by 26.66%, left bending decreased by 32.69%, right bending decreased by 21.13%, left rotation decreased by 37.34%, and right rotation decreased by 35.45% (Fig. 4).

Biconcave deformity

Stress changes in fractured vertebral body

In the biconcave deformity model, the fracture is T11 vertebral body, and the adjacent vertebral bodies are the T10 and T12 vertebral bodies. The stress distribution cloud diagram of T10, T11, and T12 vertebral bodies is shown below (Fig. 5). Under six different physiological movements of the vertebral body, the maximum stress on the T11 vertebral body before PPVA was generated by right bending, which was 23.774Mpa, while the maximum stress was the smallest generated by forward flexion, which was 19.137Mpa (Table 3). The maximum stress of the T11 vertebral body after PPVA was generated by posterior extension, which was 25.134Mpa, while the maximum stress was the smallest generated by forward flexion, which was 18.708Mpa (Table 3). After PPVA, the maximum stress of the T11 vertebral body with biconcave deformity increases except for forward flexion and left bending. Forward flexion decreased by 2.22%, posterior extension increased by 27.29%, left bending decreased by 7.47%, right bending increased by 2.41%, left rotation increased by 16.6%, and right rotation increased by 10.47% (Fig. 6).

Stress changes in adjacent vertebral bodies

Under six different physiological movements of the vertebral body, the maximum stress on the T10 vertebral body before PPVA was generated by posterior extension, which was 37.406Mpa, while the maximum stress was the smallest generated by left bending, which was 31.73Mpa (Table 3). The maximum stress of the T10 vertebral body after PPVA was also generated by posterior extension, which was 33.341Mpa, while the maximum stress was the smallest generated by forward flexion, which was 26.197Mpa (Table 3). After PPVA, the maximum stress of adjacent vertebral body T10 decreased, especially during forward flexion, which decreased by 27.95%, posterior extension decreased by 10.87%, left bending decreased by 7.29%, right bending decreased by 13.71%, left rotation decreased by 11.92%, and right rotation decreased by 13.12% (Fig. 6). Under six different physiological movements of the vertebral body, the maximum stress on the T12 vertebral body before PPVA was generated by posterior extension, which was 26.623Mpa,

Fig. 5 Stress distribution cloud diagram of biconcave deformity vertebral body and adjacent vertebral bodies before and after PPVA. Pre, Preoperative; Post, Postoperative

Table 3 Biconcave deformity vertebral body and adjacent vertebral bodies stress before and after PPVA

	Flexion		Extension		Left bending		Right bending		Left rotation		Right rotation	
	Pre	Post	Pre	Post	Pre	Post	Pre	Post	Pre	Post	Pre	Post
T10	36.361	26.197	37.406	33.341	31.73	29.416	32.495	28.041	31.956	28.145	32.093	27.882
T11	19.137	18.708	19.745	25.134	21.259	19.672	23.774	24.346	19.173	22.356	19.607	21.66
T12	21.474	23.629	26.623	25.426	24.447	27.58	23.71	24.126	24.225	24.459	23.892	24.517

Pre Preoperative, *Post* Postoperative

Fig. 6 Stress changes in biconcave deformity vertebral body and adjacent vertebral bodies under six physiological movements after PPVA

while the maximum stress was the smallest generated by forward flexion, which was 21.474Mpa (Table 3). The maximum stress of the T11 vertebral body after PPVA was generated by left bending, which was 27.58Mpa, while the maximum stress was the smallest generated by forward flexion, which was 23.629Mpa (Table 3). After PPVA, the maximum stress of adjacent vertebral body T12 was decreased by 4.5% in posterior extension, while forward flexion increased by 10.04%, posterior extension decreased by 4.5%, left bending increased by 12.82%, right bending increased by 1.75%, left rotation increased by 0.97%, and right rotation increased by 2.62% (Fig. 6).

Collapse deformity

Stress changes in collapse deformity vertebral body

In the collapse deformity model, the fracture is in the T12 vertebral body, and the adjacent vertebral bodies are the T11 and L1 vertebral bodies. The stress distribution cloud diagram of the T12, T11, and L1 vertebral bodies is shown below (Fig. 7). Under six different physiological movements of the vertebral body, the maximum stress on the T12 vertebral body before PPVA was generated by forward flexion, which was 19.274Mpa, while the maximum stress was the smallest generated by left bending, which was 15.804Mpa (Table 4). The maximum stress of the T12 vertebral body after PPVA was also generated by forward flexion, which was 17.848Mpa, while the maximum stress was the smallest generated by right bending, which was 14.409Mpa (Table 4). After PPVA, the stress of the collapsed deformed vertebral body T12 decreased under six physiological movements, with forward flexion decreased by 7.4%, posterior extension decreased by 17.39%, left bending decreased by 3.52%, right bending decreased by 23.07%, left rotation decreased by 7.01%, and right rotation decreased by 3.71% (Fig. 8).

Fig. 7 Stress distribution cloud diagram of collapse deformity vertebral body and adjacent vertebral bodies before and after PPVA. Pre, Preoperative; Post, Postoperative

Table 4 Collapse deformity vertebral body and adjacent vertebral bodies stress before and after PPVA

	Flexion		Extension		Left bending		Right bending		Left rotation		Right rotation	
	Pre	Post	Pre	Post	Pre	Post	Pre	Post	Pre	Post	Pre	Post
T11	35.524	25.625	25.348	24.241	33.791	28.802	28.304	22.48	28.962	24.036	29.028	22.451
T12	19.274	17.848	18.036	14.9	15.804	15.248	18.731	14.409	16.334	15.189	16.21	15.609
L1	13.643	20.673	16.911	16.781	15.284	16.464	15.952	15.939	14.326	17.504	15.074	18.061

Pre Preoperative, *Post* Postoperative

Fig. 8 Stress changes in biconcave deformity vertebral body and adjacent vertebral bodies under six physiological movements after PPVA

Stress changes in adjacent vertebral bodies

Under six different physiological movements of the vertebral body, the maximum stress on the T11 vertebral body before PPVA was generated by forward flexion, which was 35.524Mpa, while the maximum stress was the smallest generated by posterior extension, which was 25.348Mpa (Table 4). The maximum stress of the T11 vertebral body after PPVA was generated by left bending, which was 28.802Mpa, while the maximum stress was the smallest generated by right rotation, which was 14.409Mpa (Table 4). After PPVA, the stress of adjacent vertebral body T11 decreased significantly during six physiological movements, with the most notable reduction observed during right rotation movements. Forward flexion decreased by 27.87%, posterior extension decreased by 4.37%, left bending decreased by 14.75%, right bending decreased by 20.58%, left rotation decreased by 17.01%, and right rotation decreased by 22.66% (Fig. 8). Under six different physiological movements of the vertebral body, the maximum stress on the L1 vertebral body before PPVA was generated by posterior extension, which was 16.911Mpa, while the maximum stress was the smallest generated by forward flexion, which was 13.643Mpa (Table 4). The maximum stress of L1 vertebral body after PPVA was generated by forward flexion, which was 20.673Mpa, while the maximum stress was the smallest generated by right bending, which was 15.939Mpa (Table 4). After PPVA, only the stress of posterior extension and right bending of adjacent vertebral body L1 decreased under six physiological movements, and the stress of right bending decreased very slightly. In addition, the stress of forward flexion increased significantly, reaching 51.53%. In other movements, posterior extension decreased by 7.68%, left bending increased by 7.72%, right bending decreased by 8.1%, left rotation increased by 22.18%, and right rotation increased by 19.82% (Fig. 8).

Discussion

The thoracolumbar vertebral body is the stage of transition from thoracic physiologic kyphosis to lumbar vertebral body physiologic lordosis. Its anatomical structure is relatively unique, making it particularly vulnerable to damage from external forces [35]. Moreover, the vertebral body undergoes degenerative changes with age, leading to vertebral body fibrosis and uneven stress distribution, resulting in high-stress concentration in certain parts of the vertebral body. More importantly, due to the decrease in bone density and quality, osteoporosis can cause changes in the shape and height of the vertebral body. As a consequence, the incidence of OVCF is often higher in the thoracolumbar spine compared to other segments of the spine [36]. VA is currently the main method for treating OVCF. Inject bone cement into the fractured vertebral body through the pedicle to alleviate pain and strengthen the vertebral body [37]. Due to differences in pedicle diameter, pedicle axis asymmetry, and potential variability or malformation of the pedicles, blood vessels, and nerves, as well as the influence of factors such as vertebral body size, mobility, and kyphosis angle. A single-pedicle approach may not achieve the expected clinical results [7–13, 38]. In addition, the abduction angle and puncture trajectory of the puncture needle mainly depend on the experience of the surgeon. However, due to the different muscle thickness of the patient's lower back and the width of the vertebral pedicle, once

the puncture position or puncture angle deviates, the puncture success rate will be affected. Therefore, we propose PPVA to treat thoracolumbar OVCF. In order to explain the surgical effect of PPVA in treating OVCF, we established a three-dimensional model using quantitative CT images of patients before and after PPVA. Six models allow us to observe better the stress conditions of the three types of OVCF. In addition, unlike previous studies that simulated bone cement into a cylindrical or spherical shape, the model used accurate intraoperative bone cement shapes, which further ensured the accuracy of the finite element model and stress data.

PPVA is modified based on the classical pedicle VA puncture. Preoperative preparation is the same as VA. The patient is kept in the prone position, the abdomen is suspended, and the C-arm X-ray locates the fractured vertebra. The design of the puncture approach was based on preoperative X-ray and CT scan images, the front and middle 1/3 of the vertebral body are used as the end point of the puncture needle and the injection point of bone cement. This area allows bone cement to diffuse from one side to the opposite side, allowing the bone cement to be well distributed within the fractured vertebral body [39]. The middle part of the vertebral body pedicle is used as a safe puncture point. Connect the puncture endpoint and the safe path point to make an extension line to the skin to serve as the skin needle entry point. Finally, the distance from the three points and the angle between the puncture path and the midline were measured. At the same time, measure the inclination angle of the puncture route and the vertebral body, the maximum inclination angle, and the minimum inclination angle to ensure that the spinal canal will not penetrate during the operation. The planned approach and inclination angle obtained were marked on the patient's body surface to facilitate intraoperative puncture. After routine disinfection and anesthesia, make a longitudinal incision of approximately 5 mm at the needle entry point in the skin puncture unilaterally into the anterior 1/3 of the vertebral body. Replace with the working cannula and push in bone cement. When the bone cement has spread to the posterior 1/3 of the vertebral body, withdraw the working casing. The above process can reduce the deflection of the bone puncture needle as much as possible during operation, and achieve maximum safety and accuracy. In addition, PPVA can to operate independently of the pedicle. During the operation, the direction and depth of the working channel can be flexibly adjusted to ensure that the bone cement is dispersed on both sides of the fractured vertebral body to the greatest extent. Avoid deviation of the needle insertion position, as the puncture needle cannot reach the target location and damage the internal wall of the pedicle, causing spinal cord or nerve damage. This approach can shorten the operation time, reduce the patient's discomfort during the operation, and improve the stability of the fractured vertebral body.

Our study focused on the von Mises stress of three different types of thoracolumbar OVCF before and after PPVA, and the results showed that in the T11 vertebral body with wedge deformity, the forward flexion position exhibited the highest von Mises stress, possibly due to the decreased height of the anterior edge of the vertebral body. The stress reduction was most prominent in the forward flexion position following the injection of bone cement into the vertebral body. In addition, PPVA also significantly improved the stress of the adjacent vertebral bodies of the deformed vertebral body. Although the stress of the T10 vertebral body during forward flexion increased, the overall stress showed a downward trend. Through stress distribution cloud diagram analysis, before PPVA, the center of the wedge deformed and adjacent vertebral bodies showed low stress levels, while the periphery showed high stress levels. However, after PPVA treatment, the stress distribution within the vertebral body became more uniform. This even stress distribution helps prevent excessive cement migration within the vertebral body and reduces the risk of vertebral body collapse [40, 41].

There is a tendency for the stress on the T11 vertebral body to increase in biconcave deformity after PPVA, especially in the extension position and left rotation. This phenomenon may be attributed to three factors. Firstly, the lower height of the center of the vertebral body contrasts with the increased height of the anterior and posterior edges. Secondly, the rigidity of the vertebral body is enhanced by the filling of bone cement. Third, the ROM of the vertebral body is the smallest during posterior extension, and due to the unique structure of the biconcave deformity and the influence of bone cement, the stress is concentrated on the posterior edge of the vertebral body. In addition, due to the increased stiffness of the vertebral body filled with bone cement, the stress on the adjacent vertebral body T12 shows an increasing trend, increasing the possibility of fracture of the T12 vertebral body [42]. On the contrary, the stress situation of adjacent vertebral body T10 was significantly improved, especially the stress during forward flexion of the vertebral body is significantly decreased. Although PPVA causes increased stress in the biconcave deformed vertebral body, it improves the stress distribution in fractured vertebral body and adjacent vertebral bodies, preventing high stress from being concentrated on one side of the vertebral body. In addition, when the biconcave deformed vertebral body and adjacent vertebral bodies are in posterior extension, the stress on the intervertebral structure is relatively more significant than in other

forms of motion but is smaller in forward flexion. Therefore, for the postoperative rehabilitation and daily life of patients with biconcave deformity, we recommend using the forward flexion position while avoiding excessive posterior extension to prevent refracture of the operative vertebral body and fracture of adjacent vertebral bodies.

PPVA significantly improved the overall stress of the collapsed deformed vertebral body T12 and adjacent superior vertebral body T11, especially the vertebral body extension and right bending movements. However, the stress on the lower vertebral body L1 exhibited a rising trend, with the most significant increase observed during forward flexion and left rotation movements, which was similar to the previous research results of Ah-Reum Cho [43]. This may be caused by the fact that the L1 vertebral body is the junction of the thoracic and lumbar vertebral bodies, and is the site of the highest concentration of stress in the whole body during activities.

In this study, we found that the stress difference between wedge deformity, biconcave deformity, and collapse deformity fractures before and after PPVA was huge. We combined relevant literature and clinical experience and found that this difference not only comes from the vertebral body morphology, but is also closely related to the patient's gender, age, osteoporosis degree, and bone cement filling [44, 45]. We used finite element analysis to prove the effectiveness of PPVA for thoracolumbar OVCF. In both wedge deformed and collapsed deformed vertebral bodies, the stress after PPVA was significantly reduced. However, for vertebral body with biconcave deformity, the effect of PPVA treatment is unsatisfactory. In addition, PPVA affects the stress of adjacent vertebral bodies of the three types of OVCF. Although the stress of the inferior vertebral body with double concave deformity and collapse deformity is increased, the stress cloud map shows that the stress distribution of the vertebral body is relatively uniform compared with that before PPVA, which avoids partial stress concentration leading to refracture. Recent studies have shown that increased stress on the adjacent vertebral bodies is a risk factor for fracture. In particular, osteoporotic vertebral bodies are susceptible to the stiffness of bone cement, whereas normal vertebral bodies do not have this concern [46]. Therefore, we recommend that OVCF patients who undergo PPVA treatment, especially those with biconcave and collapsed vertebral bodies, receive a certain period of anti-osteoporosis treatment after surgery.

There are some limitations to the study. Firstly, this study mainly observed the overall stress of the vertebral body at the macro level, the same material properties were used to establish the models, without taking into account individual differences in patient gender, age, and osteoporosis degree. Secondly, the finite element model is established based on the patient's own CT imaging data, which may limit the breadth and representativeness of the model. Therefore, it cannot represent that PPVA has the same surgical effect on different patients with the same fracture type. In the future, the sample size needs to be expanded. Thirdly, since the establishment of the model is directly based on the patient's CT data, there is no comparison with the normal vertebral body model to verify the validity of the model. Fourthly, In this study, the stress changes of the vertebral body were mainly observed. In order to ensure data management, the model established was relatively simplified and the specific parameters of the intervertebral disc proposed by Niemeyer et al. [47] were not used for accurate modeling. Fifthly, the stress situation of the finite element model uses the normal physiological motion state of the vertebral body under ideal conditions, which cannot truly simulate the mechanical environment of the human body in daily life, and further biomechanical research is needed. In addition, the results of the finite element analysis can only explain the stress on the vertebral body in the short term after surgery, and cannot predict the long-term clinical effects. Therefore, in the future, we will focus on long-term follow-up of patients. Our purpose is to propose a new VA idea for treating OVCF in the thoracolumbar segment, and we will conduct more research in the future to further improve the efficacy of treating OVCF.

Conclusion

In summary, PPVA shows positive surgical results in the treatment of wedge-shaped and collapsed deformed vertebral bodies, although its effectiveness in the treatment of biconcave vertebral bodies is limited. However, this still provides a reference basis for the clinical use of PPVA to treat OVCF. According to each patient's specific case and imaging data, an individualized puncture route can be developed to improve the puncture success rate and increase the quality of the operation.

Abbreviations

CT	Computed Tomography
OVCF	Osteoporotic Vertebral Compression Fracture
PPVA	Precise Puncture Vertebral Augmentation
PKP	Percutaneous Kyphoplasty
PVP	Percutaneous Vertebroplasty
ROM	Range of Motion
VA	Vertebral Augmentation

Acknowledgements

Not applicable.

Authors' contributions

Conception and study design: Hongyu Pan, Hongtao Li, Changming Xiao and SenLi; acquisition of data: Hongyu Pan, Hongtao Li, Changming Xiao; analysis and interpretation of data: Hongyu Pan, Hongtao Li, Changming Xiao; drafting of manuscript: Hongyu Pan, Hongtao Li, Tianzhu Liu; critical revision: Hongyu Pan, Hongtao Li, Tianzhu Liu, Changming Xiao, SenLi. All authors commented

on previous versions of the manuscript. All authors read and approved the final manuscript.

Funding
This work received funding from the Drum Tower Hospital Talent Introduction Fund (RC2023-040), and Clinical Trials from the Affiliated Drum Tower Hospital, Medical School of Nanjing University (2024-LCYJ-PY-53).

Availability of data and materials
The datasets used and/or analyzed during the current study are available from the corresponding author upon reasonable request.

Declarations

Ethics approval and consent to participate
This study obtained an exemption from ethical approval from the Ethics Committee of the Affiliated Hospitalof Traditional ChineseMedicine of Southwest Medical University due|to the use of anonymized data: in accordance with the Declaration of Helsinki. The authors obtained informed consent from the patients.

Consent for publication
Informed consent was obtained from all patients.

Competing interests
The authors declare no competing interests.

Author details
[1]Department of Spinal Surgery, The Affiliated Traditional Chinese Medicine Hospital, Southwest Medical University, Luzhou, Sichuan, China. [2]Division of Spine Surgery, Department of Orthopedic Surgery, Nanjing Drum Tower Hospital, Affiliated Hospital of Medical School, Nanjing University, Nanjing, Jiangsu, China. [3]Neurological Disease Center, Zigong Fourth People's Hospital, Zigong, Sichuan, China.

Received: 25 May 2024 Accepted: 25 July 2024
Published online: 30 July 2024

References

1. Lin X, Xiong D, Peng YQ, Sheng ZF, Wu XY, Wu XP, Wu F, Yuan LQ, Liao EY. Epidemiology and management of osteoporosis in the People’s Republic of China: current perspectives. Clin Interv Aging. 2015;0(0):1017–1017. https://doi.org/10.2147/cia.s54613
2. Martikos K, Greggi T, Faldini C, Vommaro F, Scarale A. Osteoporotic thoracolumbar compression fractures: long-term retrospective comparison between vertebroplasty and conservative treatment. Eur Spine J. 2018;27(S2):244–7. https://doi.org/10.1007/s00586-018-5605-1.
3. Zhang L, Zhai P. A comparison of percutaneous vertebroplasty versus conservative treatment in terms of treatment effect for osteoporotic vertebral compression fractures: a meta-analysis. Surg Innov. 2019;27(1):19–25. https://doi.org/10.1177/1553350619869535.
4. Patel D, Liu J, Ebraheim NA. Managements of osteoporotic vertebral compression fractures: a narrative review. World J Orthop. 2022;13(6):564–73. https://doi.org/10.5312/wjo.v13.i6.564.
5. Liu H, Deng L, Zhang J, Zhou Q, Zhou Q, Fan C-Y, Chen K, Yang H. Effect of different anesthesia and puncture methods of percutaneous kyphoplasty on more than 90-year-old osteoporotic vertebral fracture: advantages of the ERAS concept. Int J Clin Pract. 2022;2022:1–8. https://doi.org/10.1155/2022/7770214.
6. Rajasekaran S, Kanna RM, Schnake KJ, Vaccaro AR, Schroeder GD, Sadiqi S, Oner C. Osteoporotic thoracolumbar fractures—how are they different?—Classification and treatment algorithm. J Orthop Trauma. 2017;31(4):S49–56. https://doi.org/10.1097/bot.0000000000000949.
7. Ozer AF, Suzer T, Can H, Falsafi M, Aydin M, Sasani M, Oktenoglu T. Anatomic assessment of variations in Kambin's triangle: a surgical and cadaver study. World Neurosurg. 2017;100:498–503. https://doi.org/10.1016/j.wneu.2017.01.057.
8. Machino M, Nakashima H, Ito K, Katayama Y, Matsumoto T, Tsushima M, Ando K, Kobayashi K. Age-related degenerative changes and sex-specific differences in osseous anatomy and intervertebral disc height of the thoracolumbar spine. J Clin Neurosci. 2021;90:317–24. https://doi.org/10.1016/j.jocn.2021.06.020.
9. Wang H, Hu P, Wu D, Zhang N, Jun W, Xiang L. Age, gender, level and side differences in the anatomical distinctions of unilateral percutaneous kyphoplasty through the transverse processpedicle approach. Pain Physician. 2019;2(22.2):E91–6. https://doi.org/10.36076/ppj/2019.22.e91.
10. Liu J-T, Li C-S, Chang C-S, Liao W-J. Long-term follow-up study of osteoporotic vertebral compression fracture treated using balloon kyphoplasty and vertebroplasty. J Neurosurg. 2015;23(1):94–8. https://doi.org/10.3171/2014.11.spine14579.
11. Pan Z, Zhou Q, Yang M, Deng L, Xiayu H, Lv N, Yang S, Yang H. Effects of distribution of bone cement on clinical efficacy and secondary fracture after percutaneous kyphoplasty for osteoporotic vertebral compression fractures. Front Surg. 2023;9. https://doi.org/10.3389/fsurg.2022.1054995.
12. Schupfner R, Koniarikova K, Pfeifer C, Grechenig P, Bakota B, Staresinic M, Kerner MA, Müller M. An anatomical study of transpedicular vs. extrapedicular approach for kyphoplasty and vertebroplasty in the thoracic spine. Injury. 2021;52(0):S63-S69. https://doi.org/10.1016/j.injury.2020.11.017.
13. Gao T, Chen ZY, Li T, Lin X, Hu HG, Yuan DC, Zeng J, Wu C. Correlation analysis of the puncture-side bone cement/vertebral body volume ratio and bone cement leakage in the paravertebral vein in vertebroplasty. BMC Musculoskelet Disord. 2022;23(1):0–0. https://doi.org/10.1186/s12891-022-05135-w.
14. Tao W, Hu Q, Nicolas YS, Nuo X, Daoyu H, Zhen J, Jinpeng S, Jun L. Is unilateral transverse process-pedicle percutaneous kyphoplasty a better choice for osteoporotic thoracolumbar fractures in the old patients?. BMC Surg. 2021;21(1):0–0. https://doi.org/10.1186/s12893-021-01246-8.
15. Zhuo Y, Liu L, Wang H, Li P, Zhou Q, Liu Y. A modified transverse process-pedicle approach applied to unilateral extrapedicular percutaneous vertebroplasty. Pain Res Manage. 2021;2021:6493712. https://doi.org/10.1155/2021/6493712.
16. Huang J, Yang J, Chen L, Xu Y, Wang S. A novel puncture approach via point "O" for percutaneous kyphoplasty in patients with L4 or L5 osteoporotic vertebral compression fracture. Sci Rep. 2022;12(1):0–0. https://doi.org/10.1038/s41598-022-23732-6.
17. Joseph Melton L, Lane AW, Cooper C, Richard Eastell W, O'Fallon M, Lawrence Riggs B. Prevalence and incidence of vertebral deformities. Osteoporos Int. 1993;3(3):113–9. https://doi.org/10.1007/bf01623271.
18. Guo W, Jiang Y, Zhu Y, Huang J. Effect of ACDF combined with different degrees of partial resection of uncovertebral joints on cervical stability and degeneration: a three-dimensional finite element analysis. J Orthop Surg Res. 2022;17(1):551. https://doi.org/10.1186/s13018-022-03447-0.
19. Yan J, Liao Z, Yu Y. Finite element analysis of dynamic changes in spinal mechanics of osteoporotic lumbar fracture. Eur J Med Res. 2022;27(1):142. https://doi.org/10.1186/s40001-022-00769-x.
20. Zhang Q, Zhang Y, Chon TE, Baker JS, Gu Y. Analysis of stress and stabilization in adolescent with osteoporotic idiopathic scoliosis: finite element method. Comput Methods Biomech Biomed Engin. 2023;26(1):12–24. https://doi.org/10.1080/10255842.2022.2044803.
21. Zhao WT, Qin DP, Zhang XG, Wang ZP, Tong Z. Biomechanical effects of different vertebral heights after augmentation of osteoporotic vertebral compression fracture: a three-dimensional finite element analysis. J Orthop Surg Res. 2018;13(1):32. https://doi.org/10.1186/s13018-018-0733-1.
22. Baroud G, Nemes J, Ferguson SJ, Steffen T. Material changes in osteoporotic human cancellous bone following infiltration with acrylic bone cement for a vertebral cement augmentation. Comput Methods Biomec Biomed Eng. 2003;6(2):133–9. https://doi.org/10.1080/1025584031000095746.
23. Böger A, Heini PF, Windolf M, Schneider E. Adjacent vertebral failure after vertebroplasty: a biomechanical study of low-modulus PMMA cement. Eur Spine J. 2007;16(12):2118–25. https://doi.org/10.1007/s00586-007-0473-0.
24. Peng Yi, Xianping Du, Huang L, Li J, Zhan R, Wang W, Biaoxiang Xu, Song Wu, Peng C, Chen S. Optimizing bone cement stiffness for vertebroplasty through biomechanical effects analysis based on patient-specific

three-dimensional finite element modeling. Med Biol Eng Compu. 2018;56(11):2137–50. https://doi.org/10.1007/s11517-018-1844-x.
25. Day GA, Jones AC, Wilcox RK. Optimizing computational methods of modeling vertebroplasty in experimentally augmented human lumbar vertebrae. JOR spine. 2020;3(1). https://doi.org/10.1002/jsp2.1077.
26. Liebschner MA, Kopperdahl DL, Rosenberg WS, Keaveny TM. Finite element modeling of the human thoracolumbar spine. Spine. 2003;28(6):559–65. https://doi.org/10.1097/01.BRS.0000049923.27694.47.
27. Mondal S, MacManus DB, Banche-Niclot F, Vitale-Brovarone C, Fiorilli S, McCarthy HO, Dunne N. Finite element analysis of vertebroplasty in the osteoporotic T11–L1 vertebral body: Effects of bone cement formulation. J Biomed Mater Res B Appl Biomater. 2024;112(1):e35359. https://doi.org/10.1002/jbm.b.35359.
28. El-Rich M, Arnoux P-J, Wagnac É, Brunet C, Aubin C-É. Finite element investigation of the loading rate effect on the spinal load-sharing changes under impact conditions. J Biomech. 2009;42(9):1252–62. https://doi.org/10.1016/j.jbiomech.2009.03.036.
29. Zuo XH, Chen YB, Xie P, Zhang WD, Xue XY, Zhang QX, Shan B, Zhang XB, Bao HG, Si YN. Finite element analysis of wedge and biconcave deformity in four different height restoration after augmentation of osteoporotic vertebral compression fractures. J Orthop Surg Res. 2021;16(1):138. https://doi.org/10.1186/s13018-021-02225-8.
30. Ogurkowska MB, Błaszczyk A. Distribution of Young's modulus at various sampling points in a human lumbar spine vertebral body. Spine J. 2020;20(11):1861–75. https://doi.org/10.1016/j.spinee.2020.06.013.
31. Daggfeldt K, Thorstensson A. The mechanics of back-extensor torque production about the lumbar spine. J Biomech. 2003;36(6):815–25. https://doi.org/10.1016/s0021-9290(03)00015-0.
32. de Zee M, Hansen L, Wong C, et al. A generic detailed rigid-body lumbar spine model. J Biomech. 2007;40(6):1219–27. https://doi.org/10.1016/j.jbiomech.2006.05.030.
33. Ehlers W, Karajan N, Markert B. An extended biphasic model for charged hydrated tissues with application to the intervertebral disc. Biomech Model Mechanobiol. 2009;8(3):233–51. https://doi.org/10.1007/s10237-008-0129-y.
34. Liang De, Ye L-Q, Jiang X, Yang P, Zhou G, Yao Z, Zhang S-C, Yang Z. Biomechanical effects of cement distribution in the fractured area on osteoporotic vertebral compression fractures: a three-dimensional finite element analysis. J Surg Res. 2015;195(1):246–56. https://doi.org/10.1016/j.jss.2014.12.053.
35. Li Q, Yun C, Li S. Transpedicular bone grafting and pedicle screw fixation in injured vertebrae using a paraspinal approach for thoracolumbar fractures: a retrospective study. J Orthop Surg Res. 2016;11(1):0–0. https://doi.org/10.1186/s13018-016-0452-4.
36. Z Wang, R Sun, SD Zhang, XT Wu. Comparison of thoracolumbar versus non-thoracolumbar osteoporotic vertebral compression fractures in risk factors, vertebral compression degree and pre-hospital back pain. J Orthop Surg Res. 2023;18(1):0-0. https://doi.org/10.1186/s13018-023-04140-6.
37. Study of unilateral extrapedicular and bilateral pedicle approach percutaneous kyphoplasty for osteoporotic vertebral compression fracture. JCPSP. J Coll Physicians Surg Pak. 2022;32(07):924–927. https://doi.org/10.29271/jcpsp.2022.07.924.
38. Chang WS, Lee S-H, Choi WG, Choi G, Jo B-J. Unipedicular vertebroplasty for osteoporotic compression fracture using an individualized needle insertion angle. Clin J Pain. 2007;23(9):767–73. https://doi.org/10.1097/ajp.0b013e318154b6c3.
39. Xiaoming Xiong Yu, Sun S-M, Yang M, Zhou J, Wan D, Deng X, Shi H. Efficacy of unilateral transverse process-pedicle and bilateral puncture techniques in percutaneous kyphoplasty for Kummell disease. Exp Ther Med. 2019. https://doi.org/10.3892/etm.2019.7980.
40. Li Y, Guo D-Q, Zhang S-C, Liang De, Yuan K, Mo G-y, Li D-X, Guo H, Tang Y-C, Luo P. Risk factor analysis for re-collapse of cemented vertebrae after percutaneous vertebroplasty (PVP) or percutaneous kyphoplasty (PKP). Int Orthop. 2018;42(9):2131–9. https://doi.org/10.1007/s00264-018-3838-6.
41. Qi J, Yuanyu Hu, Yang Z, Dong Y, Zhang X, Hou G, Lv Y, Guo Y, Zhou F, Liu B, Tian Y. Incidence, risk factors, and outcomes of symptomatic bone cement displacement following percutaneous kyphoplasty for osteoporotic vertebral compression fracture: a single center study. J Clin Med. 2022;11(24):7530–7530. https://doi.org/10.3390/jcm11247530.
42. Song Q, Zhao Y, Liu D, Liu Z, Zhang Y, Shang D, Geng Z, Shi Z, Fan L. Effect of different bone cement distributions in percutaneous kyphoplasty on clinical outcomes for osteoporotic vertebral compression fractures: a retrospective study. Medicine. 2023;102(12):e33309–e33309. https://doi.org/10.1097/md.0000000000033309.
43. Cho AR, Cho SB, Jae-Ho L, Kim KH. Effect of augmentation material stiffness on adjacent vertebrae after osteoporotic vertebroplasty using finite element analysis with different loading methods. Pain physician. 2015;18(6):E1101-10.
44. Kim Y-Y, Rhyu K-W. Recompression of vertebral body after balloon kyphoplasty for osteoporotic vertebral compression fracture. Eur Spine J. 2010;19(11):1907–12. https://doi.org/10.1007/s00586-010-1479-6.
45. Zuo XH, Chen YB, Xie P, Zhang WD, Xue XY, Zhang QX, Shan B, Zhang XB, Bao HG, Si YN. Finite element analysis of wedge and biconcave deformity in four different height restoration after augmentation of osteoporotic vertebral compression fractures. J Orthop Surg Res. 2021;16(1):0–0. https://doi.org/10.1186/s13018-021-02225-8.
46. Mills ES, Hah RJ, Fresquez Z, Mertz K, Buser Z, Alluri RK, Anderson PA. Secondary fracture rate after vertebral osteoporotic compression fracture is decreased by anti-osteoporotic medication but not increased by cement augmentation. J Bone Joint Surg Am. 2022;104(24):2178–85. https://doi.org/10.2106/jbjs.22.00469.
47. Niemeyer F, Wilke HJ, Schmidt H. Geometry strongly influences the response of numerical models of the lumbar spine–a probabilistic finite element analysis. J Biomech. 2012;45(8):1414–23. https://doi.org/10.1016/j.jbiomech.2012.02.021.

Publisher's Note